Rogue nanowaves: A route to film rupture

James E. Sprittles [1,*] Jingbang Liu [1,†] Duncan A. Lockerby [2,‡] and Tobias Grafke [1,§]
^{1}*Mathematics Institute, Zeeman Building, University of Warwick, Coventry CV4 7AL, United Kingdom*
^{2}*School of Engineering, University of Warwick, Coventry CV4 7AL, United Kingdom*

Sufficiently thin liquid films on solid surfaces are often unstable to intermolecular forces and it is commonly assumed that their rupture occurs via a linear instability mechanism in the so-called spinodal regime. Here, a theoretical framework is created for the experimentally observed thermal regime, in which fluctuation-induced nanowaves rupture linearly stable films. Molecular simulations in a quasi-2D geometry identify these regimes and are accurately reproduced by stochastic simulations based on fluctuating hydrodynamics. Rare-event theory is then applied to, and developed for, this field to provide exceptional computational efficiency and accuracy that allows us to extend calculations deep into the thermal regime. Analysis of the rare-event theory reveals a picture of how and when "rogue nanowaves" are able to provide a route to film rupture. Finally, future applications of the new theoretical framework and experimental verification is discussed.

I. INTRODUCTION

The stability of thin layers of liquid on solids is crucial for a myriad of technological applications of fluids, such as nanomanufacturing (e.g., of thin-film solar cells) [1], tear films and "dry out" of the eye [2], and bionic nanodevices for regenerative medicine [3]. As the height h^* (∗ denotes dimensional quantities) of these films approaches the nanoscale (Fig. 1), physical effects that are negligible at conventional engineering scales come into play [4–6]. Specifically, strong nonlocal interactions of molecules of the solid and liquid [7,8] can drive film rupture ($h^* = 0$ at a point) and subsequently dewet the solid.

Theoretically, the forces that can destabilize thin liquid films are often modeled by a disjoining pressure $\Pi^* = -A^*/6\pi h^{*3}$ [7,9], where A^* is the Hamaker constant associated with the solid-liquid-vapor system. Then, for a film of length L^*, assumed periodic to enable comparisons to molecular dynamics (MD), balancing (destabilizing) disjoining pressure with (stabilizing) surface tension γ^* shows that films need to be thinner than $H^* = \sqrt[4]{A^*(L^*)^2/(8\pi^3\gamma^*)}$ to be linearly unstable [10–12]—this allows unstable waves to "fit" within the domain. Early experiments [13] seemingly confirmed the theoretical discovery of this "spinodal" regime of rupture.

---

*J.E.Sprittles@Warwick.ac.uk
†Jingbang.Liu@Warwick.ac.uk
‡Duncan.Lockerby@warwick.ac.uk
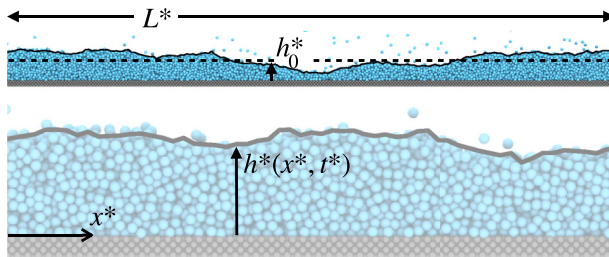§T.Grafke@Warwick.ac.uk

FIG. 1. Schematic of our setup, with the upper panel showing a periodic MD domain of length L^*, containing a film of average/initial-flat height h_0^*. The lower panel shows a close up, with the free surface extracted from the MD and the evolving local height $h^*(x^*, t^*)$.

From the late 1990s onwards, novel experimental setups were focused on the breakup of these "ultrathin" films [14–18], with discoveries of different breakup morphologies and clarification of how film/substrate defects can create a "nucleation regime" of breakup [18,19]. To understand these findings, computation of thin-film models, augmented with a disjoining pressure [20,21], were deployed to rationalize the dewetting patterns observed within the spinodal regime [22–25], i.e., for initial film heights $h_0^* < H^*$. Interestingly, this impressive body of work showed that thermal fluctuations also have a role to play in the breakup; in (i) "speeding up" the spinodal breakup ($h_0^*/H^* < 1$) to bring theory in line with experiments [26,27] and (ii) creating a new "thermal regime" of breakup [18] that can be observed for a linearly stable film ($h_0^*/H^* > 1$), as shown experimentally in [18] by using two-layer solids to modulate H^*.

In thermal equilibrium, it has long been known that thermal (Brownian) motion within the bulk of a liquid creates waves at a confining interface which "roughen" it [28,29], and that a length scale associated with this roughening is $\ell_T^* = \sqrt{k_B^* T^*/\gamma^*} \sim$ nm for typical fluids (i.e., they are nanowaves). This has been confirmed by scattering experiments [30,31] and, relatively recently, by direct visual observations using ultralow surface-tension fluids, with $\ell_T^* \sim$ μm, in various configurations [32–36]. Intriguingly, despite this progress, there is still no theoretical framework for the "thermal regime," where large, or "rogue," nanowaves appear to be able to rupture thin films; this is the focus of our Letter.

Whilst experiments can access some insight into life at the nanoscale, often utilizing complex fluid and/or solid arrangements [18,32], such observations are typically very challenging. An alternative approach, taken here, is to use MD as a virtual nanoscale experiment.

II. MOLECULAR SIMULATIONS

To build a framework for the thermal regime, we begin by considering a quasi-2D geometry (Fig. 1), with periodicity enforced over a short length $L_y^* = 3.14$ nm "into the page" will be useful for building a simplified picture of the phenomenon before extending it to 3D in future work, as discussed later. We consider a thin film of Lennard-Jones liquid at temperature $T^* = 85$ K and viscosity $\mu^* = 3.1 \times 10^{-4}$ kg/(ms). The liquid is at equilibrium with its own vapour, with interfacial tension $\gamma^* = 0.016$ N/m, and is sat on a thick atomic solid. All interactions are described by a Lennard-Jones potential, with $A^* = A_{ls}^* - A_{ll}^* \approx -1.9 \times 10^{-20}$ J—see Supplemental Material (SM1) [37] for further details (notably, within the SM we also introduce references [38–45]). Quantities are periodic on $x^* \in [0, L^*]$ and we used two domain lengths, $L^* = 19.6, 80$ nm, for which $H^* = 1.16, 2.35$ nm.

Figure 2 shows that, as hinted at in previous molecular simulations [46,47], MD predicts a thermal regime, breaking a linearly (and thus, conventionally) stable film in which $h_0 \equiv h_0^*/H^* > 1$.

Due to the stochastic nature of the thermal regime, rupture must now be characterized statistically. In particular, we record h at the rupture time τ [requiring $\min_x h(x, \tau) = 0$], center the rupture
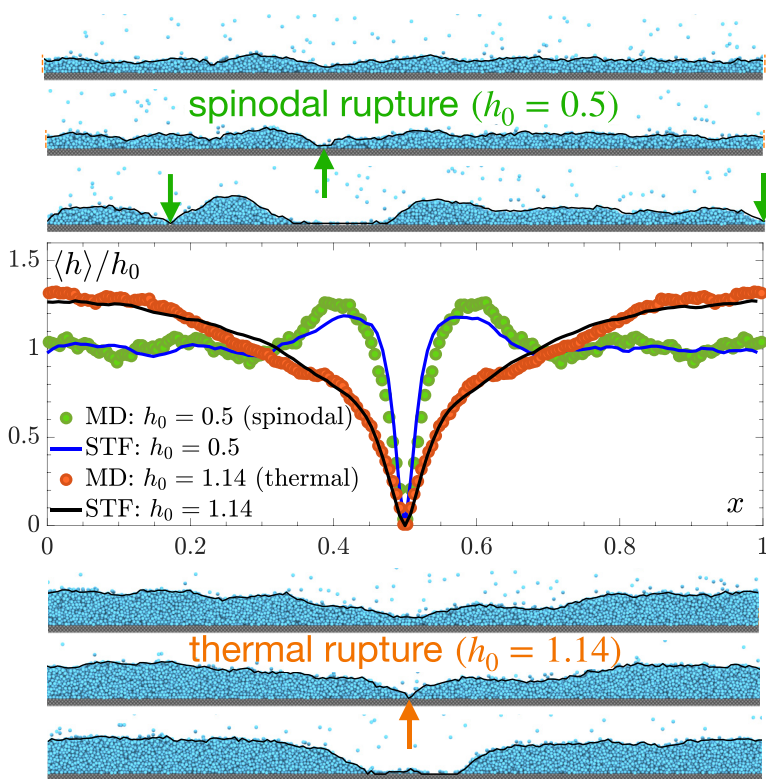
FIG. 2. Snapshots from the molecular simulations as rupture is approached in the spinodal (upper) and thermal (lower) regimes for thin films of length $L^* = 80$ nm, for which $H^* = 2.35$ nm. Arrows denote rupture points. The central figure shows a comparison of ensemble-averaged profiles $\langle h \rangle$ from the MD and stochastic thin film equation (STF) for these cases. Symmetry about $x = 1/2$ is used to further average the MD profile. Videos of these cases are provided as Supplemental Material and described in SM3.

at $x = 1/2$, and then ensemble average to find $\langle h(x, \tau) \rangle$, as shown in Fig. 2. The average time it takes for rupture to occur $\langle \tau \rangle$ is presented in Fig. 3 (symbols represent MD in both figures). Deep within the spinodal regime ($h_0 = 0.5$), the qualitative picture of growing unstable waves creating multiple localized rupture points is borne out in Fig. 2 by (i) the snapshots shown (from a single realisation), which contains three rupture points; and (ii) the ensemble-averaged profile, where a rim appears either side of the break point to conserve mass locally, with little disturbance to the film further away (i.e., $\langle h \rangle / h_0 \approx 1$ there). In contrast, in the thermal regime ($h_0 = 1.14$), there is (i) a single rupture point and (ii) the entire free surface is deformed, so that $\langle h \rangle / h_0 > 1$ far from the rupture point.

For the rupture times in Fig. 3, the MD shows a rapid increase of $\langle \tau \rangle$ with h_0 in the thermal regime, to the extent that the rupture time quickly exceeds those which can be computed within MD (i.e., dimensionally, times $\gtrsim \mu$s), even in this simplified quasi-2D setting.

The MD naturally captures the relevant nanoscale physics, but has the drawback of both being computationally intensive, particularly when considering application-scale (and inherently 3D) film sizes and timescales, and providing little qualitative understanding of the dominant underlying physics. This motivates the development of macroscopic theory for this class of flows which (i) incorporates the dominant physical mechanisms, (ii) can be validated against MD, and (iii) naturally extends to larger scales.
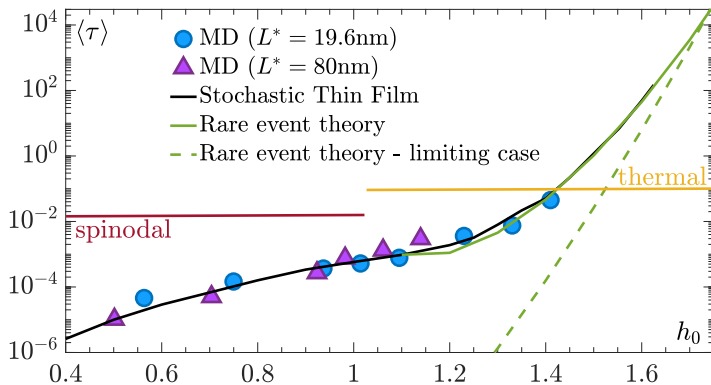
FIG. 3. Dependency of the expected rupture time $\langle\tau\rangle$ as a function of film height h_0; comparing MD data for two domain sizes with the stochastic thin-film equation and rare-event theory. For the MD, $\pm$ one standard error fits within the data point.

III. FLUCTUATING HYDRODYNAMICS

To incorporate thermal fluctuations into macroscopic fluid dynamics, Landau and Lifshitz supplemented the Navier Stokes equations with a "noisy" stress tensor [48,49], to create the field of fluctuating hydrodynamics. Early applications to interfacial flows were to the breakup of nanojets [50–53], after which a stochastic thin-film equation (STF) was derived for films on solids [54,55], which has subsequently found wide applicability [56–60]. Notably, previous analyses have shown that the STF describes MD at, and during the approach to, thermal equilibrium [40,61,62].

The STF describes a film height $h^*(x^*, t^*)$, and to compare to MD we consider a quasi-2D situation with all quantities averaged over the (short) length L_y^* "into the page," and periodic on $x^* \in [0, L]$. Nondimensionalizing the film height with respect to H^*, lateral lengths with respect to L^*, and time with $3\mu^*(L^*)^4/(\gamma^*(H^*)^3)$, we obtain a dimensionless STF

$$\frac{\partial h}{\partial t} = \frac{\partial}{\partial x}\left[m(h)\frac{\partial p}{\partial x} + \sqrt{2\epsilon m(h)}\eta\right], \quad p = -\frac{\partial^2 h}{\partial x^2} + \frac{4\pi^2}{3h^3} \tag{1}$$

in a domain [0,1) with initial height $h = h_0$, mobility $m(h) = h^3 + \ell h^2$, with $\ell = \ell^*/H^*$ the slip length ($\ell = 0$, i.e., no slip, is used initially); and a parameter $\epsilon = (\ell_T^*/H^*)^2(L^*/L_y^*)$ denoting the "noise strength." Notably, the pressure contains contributions from both the surface tension and standard disjoining pressure term. The noise is uncorrelated in space and time:

$$\langle\eta_i(x, t)\eta_j(x', t')\rangle = \delta_{ij}\delta(t - t')\delta(x - x'). \tag{2}$$

In fact, ϵ is independent of L^* (as $H^* \sim \sqrt{L^*}$) and for our molecular simulations we have $\epsilon = 0.34$. Notably, in thermal equilibrium (assuming negligible disjoining pressure) the standard deviation of the fluctuations around $h = h_0$ can be shown to be $\sigma = \sqrt{\epsilon/12}$, so that ϵ is related to the characteristic amplitude of the nanowaves. Details of the STF computations are provided in the SM where we justify the use of a simplified (but still nonlinear) STF with constant mobility $m(h) = h_0^3 + \ell h_0^2$, which is used throughout this Letter. This allows for faster computations, using exponential time differencing [63] to tackle the stiffness of the STF, to reveal significantly more of the thermal regime (see the SM2). Ensemble averaging of the STF is over 100 realizations.

In the spinodal regime ($h_0 = 0.5$), Fig. 2 shows that ensemble-averaged STF and MD profiles agree favorably, with both showing disturbances/waves either side of the rupture point that are reminiscent of those observed in [23], where these perturbations trigger secondary rupture events. This is supported by the MD realization shown. However, the influence of thermal fluctuations in the spinodal regime is well known [27] and not our main focus.

In the thermal regime ($h_0 = 1.14$), the STF is able to predict rupture and the profiles again agree remarkably well with those from MD. Furthermore, Fig. 3 shows that the STF predictions cut through the MD data over more than three orders of magnitude in $\langle \tau \rangle$. Whilst the STF extends past the MD by over two orders of magnitude in $\langle \tau \rangle$, as this approaches 10^2 the number of computational time steps for each of the 100 realizations is $\sim 10^9$, so that this Monte Carlo sampling approach becomes computationally infeasible.

IV. RARE-EVENT THEORY

Within the thermal regime, rupture is observed when fluctuation-induced nanowaves drive the interface into configurations that are unstable to the influence of disjoining pressure. Mathematically, then, we have finite-size perturbations that are pushing the interface through a saddle point $h_s(x)$ separating stable from unstable film profiles. When the energy (to fight against surface tension) required to reach this saddle point is significant, a large deviation principle often holds [64], so that we can exploit knowledge from the traditionally segregated field of rare events. There, infeasible Monte Carlo sampling computations are replaced by tractable deterministic saddle point and/or optimization calculations, with methods originally developed for quantum physics [65] and recently applied to turbulence [66,67]. Of particular note are the prediction of rogue ocean waves [68,69] using these techniques, we are interested in rogue nanowaves.

Our case is a relatively simple one; as the STF can be recast in gradient form [58],

$$\frac{\partial h}{\partial t} = -M(h)\frac{\delta U(h)}{\delta h} + \sqrt{2\epsilon}\sigma(h)\eta \tag{3}$$

with energy U and mobility operator M given by

$$U(h) = \int_0^1 \left(\frac{1}{2}\left(\frac{\partial h}{\partial x}\right)^2 - \frac{2\pi^2}{3h^2} \right)dx, \quad M(h) = -\frac{\partial}{\partial x}\left(h^3 \frac{\partial \circ}{\partial x} \right), \tag{4}$$

with $\circ$ showing what is operated on and the noise operator $\sigma(h)$ given by $\sigma(h) = \frac{\partial(h^{3/2}\circ)}{\partial x}$, so that detailed balance is satisfied (as $\sigma^\dagger = -h^{3/2}\frac{\partial \circ}{\partial x}$ and thus $\sigma\sigma^\dagger = M$).

This is a classical case covered by Kramer's law [70,71], where we would like to find the relevant saddle $h_s(x)$ of the potential U with the lowest energy $U(h_s)$, which separates stable and unstable profiles. Then, Kramer's law posits that the mean first passage time $\langle \tau \rangle$, in our case the expected rupture time, fulfills

$$\langle \tau \rangle = C e^{\epsilon^{-1}(U(h_s) - U(h_0))}. \tag{5}$$

Therefore, the path to the saddle point is unimportant in this case (extensions are discussed later), as all that matters is the energy required to reach the saddle point $U(h_s) - U(h_0)$, and our focus turns to calculating the saddle point profile so we can obtain $U(h_s)$. Interestingly, we have derived an approach which has been classically used in a similar form in [72,73] to predict experimental observations of the stability of wetting layers [74,75].

We seek to minimize U using the gentlest ascent dynamics (GAD) developed in [76], subject to mass conservation $\int_0^1 (h - h_0)\, dx = 0$ and periodicity. The results are shown in Fig. 4 where, as we expected, the calculated saddle-point profiles become increasingly deformed, so that $U(h_s)$ increases, with larger h_0. The inset of Fig. 4 considers the ensemble-averaged STF profiles obtained when conditioning on the minimum of h reaching that of the saddle. Reassuringly, for a fixed h_0, these profiles converge to the GAD-obtained saddle point shape as $\epsilon \to 0$.

In addition, we have managed to derive the prefactor (C in (5)), see [77], in a manner similar to the Eyring-Kramer formula [70]. Due to conservation of mass, the mobility operator $M(h)$ is
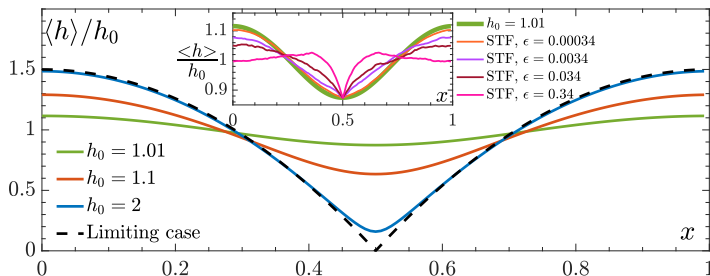
FIG. 4. Saddle-point profiles showing larger deformation as h_0 increases, approaching the limiting case (a parabola), in which disjoining pressure is negligible. Inset figure shows the saddle point for $h_0 = 1.01$ and that ensemble-averaged STF calculations converge toward this state as $\epsilon \to 0$.

degenerate, requiring extensions to the conventional formula with the prefactor C now given by

$$C = \frac{\pi}{\mu_-}\sqrt{\frac{n_s^\mathsf{T} H^{-1}(h_s)n_s}{n_0^\mathsf{T} H^{-1}(h_0)n_0}}\sqrt{\frac{\det H(h_s)}{\det H(h_0)}}, \tag{6}$$

where $H(h) = \delta^2 U/\delta h^2$ is the Hessian of the energy $U(h)$, μ_- is the only negative eigenvalue of $H(h_s)M(h_s)$, n_s is the zero eigenvector of $M(h_s)$, and n_0 is the zero eigenvector of $M(h_0)$. Interestingly, if we assume a constant mobility, the prefactor becomes

$$C = \frac{\pi}{\left(h_0^3 + lh_0^2\right)D(h_0)}\sqrt{\frac{n_0^\mathsf{T} H^{-1}(h_s)n_0}{n_0^\mathsf{T} H^{-1}(h_0)n_0}}\sqrt{\frac{\det H(h_s)}{\det H(h_0)}}, \tag{7}$$

where D is a function of h_0. This implies for a given initial film height, increasing slip length reduces the average rupture time.

Agreement between the rare-event theory and STF computations in Fig. 3 is remarkably good. The associated curves are not only graphically indistinguishable for $h_0 > 1.4$, but surprisingly, the rare-event theory is accurate right down to $h_0 \approx 1.1$. As there are no fitting parameters in the rare-event theory, this means that almost throughout the thermal regime this theory can be used to rapidly predict rupture times, including for larger values of $h_0 > 1.6$ where basic STF computations become infeasible.

As h_0 increases we can envisage a "fluctuation-dominated" regime, where disjoining pressure is negligible (except very close to the rupture event) so the system is stable to almost all finite-sized perturbations that don't instantly rupture the film. In this limiting case, the saddle point disappears, so instead we must impose a rupture point $h(1/2) = 0$ and then minimize U. Here, there is an analytic rupture profile, a parabola, given by

$$h_{\text{lim}} = 6h_0\left|x - \tfrac{1}{2}\right|\left(1 - \left|x - \tfrac{1}{2}\right|\right) \quad \text{and} \quad U = 6h_0^2, \tag{8}$$

which, in particular, has a corner at $x = 1/2$. Figure 4 shows that the saddle point profiles do indeed approach this limiting case. Here, the expected rupture time is $\langle\tau\rangle \sim e^{6h_0^2/\epsilon}$ and Fig. 3 shows that the full rare-event theory approaches this limiting case with increasing h_0.

The limiting case of the rare-event theory provides a simple picture of rupture in the thermal regime. The exponent in the expected rupture time can be rewritten as $6(h_0/\epsilon^{1/2})^2 = \tfrac{1}{2}(h_0/\sigma)^2$, which shows how the event becomes increasingly rare as the film height h_0 exceeds the characteristic amplitude of the waves in thermal equilibrium σ—where the only route to film rupture is via a rogue nanowave. Furthermore, the theory explains the MD-observed nonlocal dynamics of rupture in the thermal regime, as the entire film is deformed in order to minimize the energy requirement of doing work against surface tension. For values of h_0 closer to one, similar traits are seen, but now disjoining pressure plays a role.
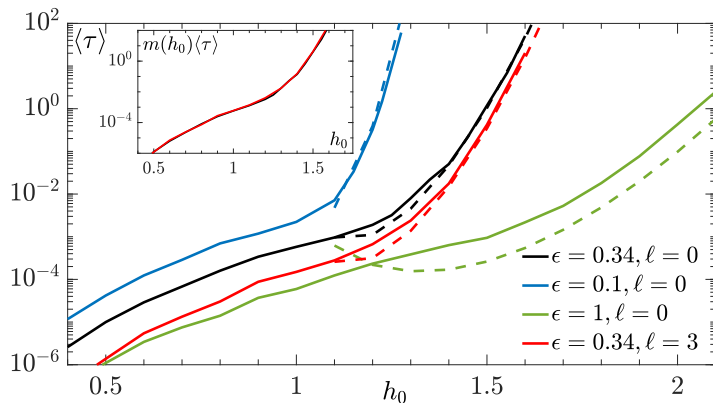
FIG. 5. Influence of the noise parameter ϵ and nonzero slip length ℓ on the expected rupture times compared to the rare-event theory. Solid lines correspond to STF calculations while dashed lines are the predictions of the rare-event theory. The inset confirms the prediction of the rare-event theory that the rupture time scales as $\sim(h_0^3 + \ell h_0^2)^{-1}$.

Notably, the transition from the thermal to spinodal regime appears smooth, e.g., in terms of $\langle\tau\rangle$ as a function of h_0, so that a more nuanced approach to classifying rupture would consider a transition region [e.g., for $h_0 \in (0.8, 1.2)$ in Fig. 3] that connects the spinodal regime, where the curve is clearly concave in Fig. 3, and the thermal one, where it becomes convex—regime signatures which should be experimentally verifiable.

In Fig. 5, it can be seen that increasing the noise strength ϵ decreases the expected rupture time for a given h_0, as one would anticipate, and that the rare-event theory can capture these trends, with better accuracy for smaller ϵ, as one would anticipate. Figure 5 also shows that introducing slip between the liquid and solid reduces the expected rupture times. This is in line with our intuition that slip increases the mobility so that fluid can more easily be pushed out of thinning regions, and therefore rupture can occur quicker. In fact, this behavior is entirely encoded in the prefactor, see (7), and the inset to Fig. 5 shows that data from different computations can be collapsed by realizing that the waiting time scales as $\sim(h_0^3 + \ell h_0^2)^{-1}$. Remarkably, in all these cases the same set of saddle-point profiles (and hence energies) can be used, with changes in ϵ altering only the denominator in the exponential and variation in ℓ changing only an algebraic part of the prefactor.

In Fig. 6, we show the distribution of rupture times $\rho(\langle\tau\rangle)$ as sampled over 1000 rupture events. Notably, for $h_0 = 1.3$, the left panel, one can clearly see an exponentially decaying behavior for $\rho(\langle\tau\rangle)$, which is further evidence of being in a rare-event regime, in which the process can be viewed as a collection of independent attempts, most of which fail to achieve rupture, and can thus be approximated as a Poisson process [78].
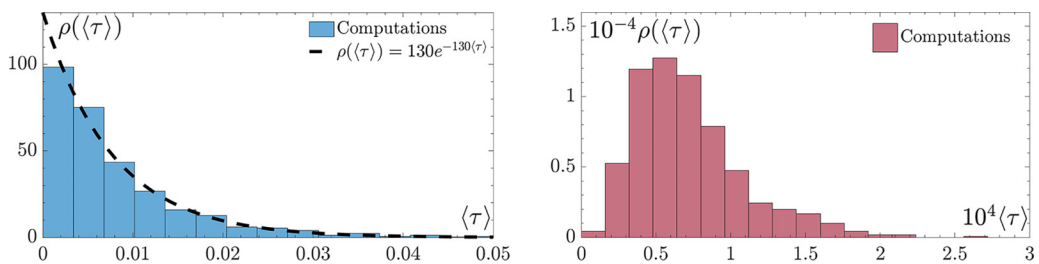

FIG. 6. Probability distribution function for 1000 computations of the rupture at $\epsilon = 0.34$ with the left panel corresponding to $h_0 = 1.3$ (thermal) and the right to $h_0 = 0.7$ (spinodal).

In contrast, in the right panel, $h_0 = 0.7$ is well within the spinodal regime and a very different distribution in Fig. 6 is observed as events are certainly no longer rare. To understand the shape of the distribution, and in particular the nonzero maxima, it becomes important to recall that the film starts from flat and the thermal waves take some time to develop. The equilibration time for the films is $\tau_{eq} \approx [\omega(k = 2\pi)]^{-1} = [(2\pi)^4 h_0^3]^{-1}$ and is much shorter than the rupture times in the thermal regime, but for this case, in the spinodal regime, it is in fact longer ($\tau_{eq} \approx 10^{-3}$) than the characteristic rupture times $\approx 10^{-4}$– this interplay between wave development and spinodal mechanisms leads to the shape shown in Fig. 6.

V. TOWARDS A COMPARISON TO THIN-FILM EXPERIMENTS

To extend the new theoretical framework beyond the limitations of MD domain sizes and toward experimental scales is relatively straightforward, as the noise parameter ϵ is independent of L^*. If we push L^* into the experimental range, say considering a $L^* = 10\,\mu$m domain, then we find dimensional scales of $H^* = 26$ nm and $T = 30$ s. Looking at Fig. 3, we see from the STF that at $h_0 = 1.5$ we have $\langle\tau\rangle \approx 1$; this implies that for a film 50% thicker than the height at which linear instability occurs (which here corresponds to $h_0^* = 39$ nm), the average rupture time is $\langle\tau^*\rangle \approx 30$ s, i.e., well within the experimental range and of important practical consequences for the stability of, e.g., liquid coatings.

Of course, most experimental systems are inherently 3D, for which the accuracy of our predictions remains to be established, with preliminary results suggesting a small scale cutoff may be needed, as seen in thermal equilibrium for the interfacial roughness [29]. Here, MD will be 3D and the STF becomes 2D; both will be significantly more computationally intensive, with large-scale computations of the STF requiring more advanced methods, such as using GPUs [79]. In 3D then, the newly validated rare-event theory will come into its own: as solutions for ensemble-averaged breakup shapes are likely to be axisymmetric, the rare-event theory can remain 1D, i.e., h_s will depend only on radius from the rupture point. Then, to describe the experiments of [18], the thermal regime must be found by using multilayer solids that create different shapes for the disjoining potential, as previously considered theoretically in [25]. Also including a repulsive term [24] will allow the subsequent dewetting to be captured and compared directly to experimental data that highlights distinct regime morphologies.

VI. FUTURE DIRECTIONS

Thermal fluctuations are known experimentally to influence a range of interfacial flows, which can now be described by the framework developed here. For example, in the breakup of "free films" that underpin the stability of bubbles/drops in foams/emulsions, thermal regimes have been observed using interferomic measurements [80], with fluctuation-enhanced colloid-polymer mixtures [34], and in MD [81]. Similarly, it will be exciting to revisit classical results on wetting layers [72,73] and soap films [82], with a framework that can capture the dynamic evolution of an interface.

Thermal activation is also crucial in low-speed dynamic wetting [83], as confirmed by MD [84] and experiments of superfluid liquid helium-4 on caesium [85,86]. Our framework could support recent theoretical work in this area [87–90] and also help to predict depinning transitions that govern the stability of nanobubbles [91,92].

An interesting case is that of nanojets, where MD and a cylindrical STF in [50] showed how fluctuations effect drop formation, as confirmed experimentally in [33]. However, here, the equations lose their gradient-flow structure, so that rare-event methods require knowledge of the entire transition path. This was formulated in [51], but only recently have methods existed to solve these so-called "instanton equations" [93,94].

Fluctuations are also crucial for nucleation/cavitation of bubbles [95–97] and ice nucleation [98]; both events sit in a rare-event regime. Notably, at such scales the surface tension can become

curvature dependent or, similarly, height dependent for thin films, if the height is comparable to the width of the confining interfaces [60,99,100] these effects could be included in future analyses.

Finally, related applications exist in other free-boundary problems. For example, those involving the interplay of fluctuations and elasticity, such as in the spreading of fluid-filled blisters [101] and transport in nanopores [102].

The data that support the findings of this study are openly available in figshare [103].

ACKNOWLEDGMENTS

[1] S. V. Makarov, V. A. Milichko, I. S. Mukhin, I. I. Shishkin, D. A. Zuev, A. M. Mozharov, A. E. Krasnok, and P. A. Belov, Controllable femtosecond laser-induced dewetting for plasmonic applications, Laser Photonics Rev. **10**, 91 (2016).

[2] R. J. Braun, Dynamics of the tear film, Annu. Rev. Fluid Mech. **44**, 267 (2012).

[3] Y. L. Kong, M. K. Gupta, B. N. Johnson, and M. C. McAlpine, 3D printed bionic nanodevices, Nano Today **11**, 330 (2016).

[4] D. Bonn, J. Eggers, J. Indekeu, J. Meunier, and E. Rolley, Wetting and spreading, Rev. Mod. Phys. **81**, 739 (2009).

[5] L. Bocquet and E. Charlaix, Nanofluidics, from bulk to interfaces, Chem. Soc. Rev. **39**, 1073 (2010).

[6] N. Kavokine, R. R. Netz, and L. Bocquet, Fluids at the nanoscale: From continuum to subcontinuum transport, Annu. Rev. Fluid Mech. **53**, 377 (2021).

[7] J. N. Israelachvili, *Intermolecular and Surface Forces* (Academic Press, San Diego, 2011).

[8] M. Rauscher and S. Dietrich, Wetting phenomena in nanofluidics, Annu. Rev. Mater. Res. **38**, 143 (2008).

[9] H. C. Hamaker, The London - van der Waals attraction between spherical particles, Physica **4**, 1058 (1937).

[10] A. Vrij, Possible mechanism for the spontaneous rupture of thin, free liquid films, Discuss. Faraday Soc. **42**, 23 (1966).

[11] E. Ruckenstein and R. K. Jain, Spontaneous rupture of thin liquid films, J. Chem. Soc., Faraday Trans. 2 **70**, 132 (1974).

[12] F. B. Wyart and J. Daillant, Drying of solids wetted by thin liquid films, Can. J. Phys. **68**, 1084 (1990).

[13] G. Reiter, Dewetting of Thin Polymer Films, Phys. Rev. Lett. **68**, 75 (1992).

[14] J. Bischof, D. Scherer, S. Herminghaus, and P. Leiderer, Dewetting Modes of Thin Metallic Films: Nucleation of Holes and Spinodal Dewetting, Phys. Rev. Lett. **77**, 1536 (1996).

[15] S. Herminghaus, K. Jacobs, K. Mecke, J. Bischof, A. Fery, M. Ibn-Elhaj, and S. Schlagowski, Spinodal dewetting in liquid crystal and liquid metal films, Science **282**, 916 (1998).

[16] R. Xie, A. Karim, J. F. Douglas, C. C. Han, and R. A. Weiss, Spinodal Dewetting of Thin Polymer Films, Phys. Rev. Lett. **81**, 1251 (1998).

[17] U. Thiele, M. Mertig, and W. Pompe, Dewetting of an Evaporating Thin Liquid Film: Heterogeneous Nucleation and Surface Instability, Phys. Rev. Lett. **80**, 2869 (1998).

[18] R. Seemann, S. Herminghaus, and K. Jacobs, Dewetting Patterns and Molecular Forces: A Reconciliation, Phys. Rev. Lett. **86**, 5534 (2001).

[19] K. Jacobs, S. Herminghaus, and K. R. Mecke, Thin liquid polymer films rupture via defects, Langmuir **14**, 965 (1998).

[20] A. Oron, S. H. Davis, and S. G. Bankoff, Long-scale evolution of thin liquid films, Rev. Mod. Phys. **69**, 931 (1997).

[21] R. V. Craster and O. K. Matar, Dynamics and stability of thin liquid films, Rev. Mod. Phys. **81**, 1131 (2009).

[22] A. Oron, Three-Dimensional Nonlinear Dynamics of Thin Liquid Films, Phys. Rev. Lett. **85**, 2108 (2000).

[23] U. Thiele, M. G. Velarde, and K. Neuffer, Dewetting: Film Rupture by Nucleation in the Spinodal Regime, Phys. Rev. Lett. **87**, 016104 (2001).

[24] J. Becker, G. Grün, R. Seemann, H. Mantz, K. Jacobs, K. R. Mecke, and R. Blossey, Complex dewetting scenarios captured by thin-film models, Nat. Mater. **2**, 59 (2003).

[25] A. Sharma, Many paths to dewetting of thin films: anatomy and physiology of surface instability, Eur. Phys. J. E **12**, 397 (2003).

[26] K. Mecke and M. Rauscher, On thermal fluctuations in thin film flow, J. Phys.: Condens. Matter **17**, S3515 (2005).

[27] R. Fetzer, M. Rauscher, R. Seemann, K. Jacobs, and K. Mecke, Thermal Noise Influences Fluid Flow in Thin Films during Spinodal Dewetting, Phys. Rev. Lett. **99**, 114503 (2007).

[28] L. Mandelstam, Íber die rauhigkeit freier flüssigkeitsoberflächen, Annalen der Physik **346**, 609 (1913).

[29] E. G. Flekkøy and D. H. Rothman, Fluctuating Fluid Interfaces, Phys. Rev. Lett. **75**, 260 (1995).

[30] A. Vrij, Light scattering from liquid interfaces, Adv. Colloid Interface Sci. **2**, 39 (1968).

[31] M. A. Bouchiat and J. Meunier, Light Scattering from Surface Waves on Carbon Dioxide Near the Critical Point, Phys. Rev. Lett. **23**, 752 (1969).

[32] D. G. A. L. Aarts, M. Schmidt, and H. N. W. Lekkerkerker, Direct visual observation of thermal capillary waves, Science **304**, 847 (2004).

[33] Y. Hennequin, D. G. A. L. Aarts, J. H. van der Wiel, G. Wegdam, J. Eggers, H. N. W. Lekkerkerker, and D. Bonn, Drop Formation by Thermal Fluctuations at an Ultralow Surface Tension, Phys. Rev. Lett. **97**, 244502 (2006).

[34] D. G. A. L. Aarts and H. N. W. Lekkerkerker, Droplet coalescence: drainage, film rupture and neck growth in ultralow interfacial tension systems, J. Fluid Mech. **606**, 275 (2008).

[35] Y. Hennequin, D. G. A. L. Aarts, J. O. Indekeu, H. N. W. Lekkerkerker, and D. Bonn, Fluctuation Forces and Wetting Layers in Colloid-Polymer Mixtures, Phys. Rev. Lett. **100**, 178305 (2008).

[36] J. Petit, D. Rivière, H. Kellay, and J.-P. Delville, Break-up dynamics of fluctuating liquid threads, Proc. Natl. Acad. Sci. **109**, 18327 (2012).

[37] See Supplemental Material at http://link.aps.org/supplemental/10.1103/PhysRevFluids.8.L092001 for a detailed description of the molecular simulations (SM1), the methods used to solve the stochastic thin film equation (SM2) and a description of the attached videos (SM3).

[38] A. P. Thompson, H. M. Aktulga, R. Berger, D. S. Bolintineanu, W. M. Brown, P. S. Crozier, P. J. in 't Veld, A. Kohlmeyer, S. G. Moore, T. D. Nguyen, R. Shan, M. J. Stevens, J. Tranchida, C. Trott, and S. J. Plimpton, LAMMPS - a flexible simulation tool for particle-based materials modeling at the atomic, meso, and continuum scales, Comput. Phys. Commun. **271**, 108171 (2022).

[39] L. Bocquet and J.-L. Barrat, Hydrodynamic boundary conditions, correlation functions, and Kubo relations for confined fluids, Phys. Rev. E **49**, 3079 (1994).

[40] Y. Zhang, D. A. Lockerby, and J. E. Sprittles, Relaxation of thermal capillary waves for nanoscale liquid films on anisotropic-slip substrates, Langmuir **37**, 8667 (2021).

[41] J. M. Haile, I. Johnston, A. J. Mallinckrodt, and S. McKay, Molecular dynamics simulation: Elementary methods, Comput. Phys. **7**, 625 (1993).

[42] A. Trokhymchuk and J. Alejandre, Computer simulations of liquid/vapor interface in Lennard-Jones fluids: Some questions and answers, J. Chem. Phys. **111**, 8510 (1999).

[43] J. H. Weijs, A. Marchand, B. Andreotti, D. Lohse, and J. H. Snoeijer, Origin of line tension for a Lennard-Jones nanodroplet, Phys. Fluids **23**, 022001 (2011).

[44] I. D. Coope, Circle fitting by linear and nonlinear least squares, J. Optim. Theory Appl. **76**, 381 (1993).

[45] A. Stukowski, Visualization and analysis of atomistic simulation data with OVITO–the Open Visualization Tool, Modell. Simul. Mater. Sci. Eng. **18**, 015012 (2010).

[46] Y. Zhang, J. E. Sprittles, and D. A. Lockerby, Molecular simulation of thin liquid films: Thermal fluctuations and instability, Phys. Rev. E **100**, 023108 (2019).

[47] T. D. Nguyen, M. Fuentes-Cabrera, J. D. Fowlkes, and P. D. Rack, Coexistence of spinodal instability and thermal nucleation in thin-film rupture: Insights from molecular levels, Phys. Rev. E **89**, 032403 (2014).

[48] L. Landau and E. Lifshitz, *Fluid Mechanics* (Pergamon Press, New York, 1959).

[49] J. M. O. de Zarate and J. V. Sengers, *Hydrodynamic Fluctuations in Fluids and Fluid Mixtures* (Elsevier, 2006).

[50] M. Moseler and U. Landman, Formation, stability, and breakup of nanojets, Science **289**, 1165 (2000).

[51] J. Eggers, Dynamics of Liquid Nanojets, Phys. Rev. Lett. **89**, 084502 (2002).

[52] C. Zhao, J. E. Sprittles, and D. A. Lockerby, Revisiting the Rayleigh-Plateau instability for the nanoscale, J. Fluid Mech. **861**, R3 (2019).

[53] C. Zhao, D. A. Lockerby, and J. E. Sprittles, Dynamics of liquid nanothreads: Fluctuation-driven instability and rupture, Phys. Rev. Fluids **5**, 044201 (2020).

[54] G. Grün, K. Mecke, and M. Rauscher, Thin-film flow influenced by thermal noise, J. Stat. Phys. **122**, 1261 (2006).

[55] B. Davidovitch, E. Moro, and H. A. Stone, Spreading of Viscous Fluid Drops on a Solid Substrate Assisted by Thermal Fluctuations, Phys. Rev. Lett. **95**, 244505 (2005).

[56] S. Nesic, R. Cuerno, E. Moro, and L. Kondic, Fully nonlinear dynamics of stochastic thin-film dewetting, Phys. Rev. E **92**, 061002(R) (2015).

[57] J. A. Diez, A. G. González, and R. Fernández, Metallic-thin-film instability with spatially correlated thermal noise, Phys. Rev. E **93**, 013120 (2016).

[58] M. A. Durán-Olivencia, R. S. Gvalani, S. Kalliadasis, and G. A. Pavliotis, Instability, rupture and fluctuations in thin liquid films: Theory and computations, J. Stat. Phys. **174**, 579 (2019).

[59] M. S. Shah, V. van Steijn, C. R. Kleijn, and M. T. Kreutzer, Thermal fluctuations in capillary thinning of thin liquid films, J. Fluid Mech. **876**, 1090 (2019).

[60] A. Alizadeh Pahlavan, L. Cueto-Felgueroso, A. E. Hosoi, G. H. McKinley, and R. Juanes, Thin films in partial wetting: stability, dewetting and coarsening, J. Fluid Mech. **845**, 642 (2018).

[61] Y. Zhang, J. E. Sprittles, and D. A. Lockerby, Nanoscale thin-film flows with thermal fluctuations and slip, Phys. Rev. E **102**, 053105 (2020).

[62] Y. Zhang, J. Sprittles, and D. Lockerby, Thermal capillary wave growth and surface roughening of nanoscale liquid films, J. Fluid Mech. **915**, A135 (2021).

[63] S. Cox and P. Matthews, Exponential time differencing for stiff systems, J. Comput. Phys. **176**, 430 (2002).

[64] M. I. Freidlin and A. D. Wentzell, *Random Perturbations of Dynamical Systems*, Grundlehren der mathematischen Wissenschaften Vol. 260 (Springer, 1998).

[65] G. 't Hooft, Computation of the quantum effects due to a four-dimensional pseudoparticle, Phys. Rev. D **14**, 3432 (1976).

[66] T. Grafke, R. Grauer, and S. Schindel, Efficient computation of instantons for multi-dimensional turbulent flows with large scale forcing, Commun. Comput. Phys. **18**, 577 (2015).

[67] G. Margazoglou, L. Biferale, R. Grauer, K. Jansen, D. Mesterházy, T. Rosenow, and R. Tripiccione, Hybrid monte carlo algorithm for sampling rare events in space-time histories of stochastic fields, Phys. Rev. E **99**, 053303 (2019).

[68] G. Dematteis, T. Grafke, and E. Vanden-Eijnden, Rogue waves and large deviations in deep sea, Proc. Natl. Acad. Sci. **115**, 855 (2018).

[69] G. Dematteis, T. Grafke, M. Onorato, and E. Vanden-Eijnden, Experimental Evidence of Hydrodynamic Instantons: The Universal Route to Rogue Waves, Phys. Rev. X **9**, 041057 (2019).

[70] H. Eyring, The activated complex in chemical reactions, J. Chem. Phys. **3**, 107 (1935).

[71] H. A. Kramers, Brownian motion in a field of force and the diffusion model of chemical reactions, Physica **7**, 284 (1940).

[72] R. Bausch and R. Blossey, Lifetime of undercooled wetting layers, Phys. Rev. E **50**, R1759 (1994).

[73] D. Bonn and J. O. Indekeu, Nucleation and Wetting near Surface Spinodals, Phys. Rev. Lett. **74**, 3844 (1995).

[74] J. E. Rutledge and P. Taborek, Prewetting Phase Diagram of He 4 on Cesium, Phys. Rev. Lett. **69**, 937 (1992).

[75] D. Bonn, H. Kellay, and G. H. Wegdam, Experimental Observation of Hysteresis in a Wetting Transition, Phys. Rev. Lett. **69**, 1975 (1992).

[76] W. E and X. Zhou, The gentlest ascent dynamics, Nonlinearity **24**, 1831 (2011).

[77] J. Liu, J. Sprittles, D. Lockerby, and T. Grafke, Mean first passage times and Eyring-Kramers formula for fluctuating hydrodynamics (unpublished).

[78] W. Feller, *An Introduction to Probability Theory and Its Applications: Volume I* (John Wiley & sons, 1968).

[79] M.-A. Y.-H. Lam, L. J. Cummings, and L. Kondic, Computing dynamics of thin films via large scale GPU-based simulations, J. Comput. Phys. **2**, 100001 (2019).

[80] E. Chatzigiannakis and J. Vermant, Breakup of Thin Liquid Films: From Stochastic to Deterministic, Phys. Rev. Lett. **125**, 158001 (2020).

[81] S. Perumanath, M. K. Borg, M. V. Chubynsky, J. E. Sprittles, and J. M. Reese, Droplet Coalescence is Initiated by Thermal Motion, Phys. Rev. Lett. **122**, 104501 (2019).

[82] V. Casteletto, I. Cantat, D. Sarker, R. Bausch, D. Bonn, and J. Meunier, Stability of Soap Films: Hysteresis and Nucleation of Black Films, Phys. Rev. Lett. **90**, 048302 (2003).

[83] T. D. Blake, The physics of moving wetting lines, J. Colloid Interface Sci. **299**, 1 (2006).

[84] J.-C. Fernández-Toledano, T. Blake, and J. De Coninck, Contact-line fluctuations and dynamic wetting, J. Colloid Interface Sci. **540**, 322 (2019).

[85] A. Prevost, E. Rolley, and C. Guthmann, Thermally Activated Motion of the Contact Line of a Liquid 4 he Meniscus on a Cesium Substrate, Phys. Rev. Lett. **83**, 348 (1999).

[86] E. Rolley and C. Guthmann, Dynamics and Hysteresis of the Contact Line between Liquid Hydrogen and Cesium Substrates, Phys. Rev. Lett. **98**, 166105 (2007).

[87] A. M. Willis and J. B. Freund, Enhanced droplet spreading due to thermal fluctuations, J. Phys.: Condens. Matter **21**, 464128 (2009).

[88] D. Belardinelli, M. Sbragaglia, M. Gross, and B. Andreotti, Thermal fluctuations of an interface near a contact line, Phys. Rev. E **94**, 052803 (2016).

[89] H. Perrin, R. Lhermerout, K. Davitt, E. Rolley, and B. Andreotti, Defects at the Nanoscale Impact Contact Line Motion at all Scales, Phys. Rev. Lett. **116**, 184502 (2016).

[90] H. Perrin, R. Lhermerout, K. Davitt, E. Rolley, and B. Andreotti, Thermally activated motion of a contact line over defects, Soft Matter **14**, 1581 (2018).

[91] D. Dockar, M. K. Borg, and J. M. Reese, Mechanical stability of surface nanobubbles, Langmuir **35**, 9325 (2019).

[92] D. Lohse and X. Zhang, Surface nanobubbles and nanodroplets, Rev. Mod. Phys. **87**, 981 (2015).

[93] T. Grafke and E. Vanden-Eijnden, Numerical computation of rare events via large deviation theory, Chaos **29**, 063118 (2019).

[94] W. E, W. Ren, and E. Vanden-Eijnden, Finite temperature string method for the study of rare events, J. Phys. Chem. B **109**, 6688 (2005).

[95] G. Menzl, M. A. Gonzalez, P. Geiger, F. Caupin, J. L. F. Abascal, C. Valeriani, and C. Dellago, Molecular mechanism for cavitation in water under tension, Proc. Natl. Acad. Sci. **113**, 13582 (2016).

[96] D. Lohse and A. Prosperetti, Homogeneous nucleation: Patching the way from the macroscopic to the nanoscopic description, Proc. Natl. Acad. Sci. **113**, 13549 (2016).

[97] M. Gallo, F. Magaletti, D. Cocco, and C. M. Casciola, Nucleation and growth dynamics of vapour bubbles, J. Fluid Mech. **883**, A14 (2020).

[98] M. Fitzner, G. C. Sosso, S. J. Cox, and A. Michaelides, Ice is born in low-mobility regions of supercooled liquid water, Proc. Natl. Acad. Sci. **116**, 2009 (2019).

[99] L. G. MacDowell, J. Benet, and N. A. Katcho, Capillary Fluctuations and Film-Height-Dependent Surface Tension of an Adsorbed Liquid Film, Phys. Rev. Lett. **111**, 047802 (2013).

[100] C. Clavaud, M. Maza-Cuello, C. Frétigny, L. Talini, and T. Bickel, Modification of the Fluctuation Dynamics of Ultrathin Wetting Films, Phys. Rev. Lett. **126**, 228004 (2021).

[101] A. Carlson, Fluctuation assisted spreading of a fluid filled elastic blister, J. Fluid Mech. **846**, 1076 (2018).

[102] S. Marbach, D. S. Dean, and L. Bocquet, Transport and dispersion across wiggling nanopores, Nat. Phys. **14**, 1108 (2018).

[103] https://doi.org/10.6084/m9.figshare.23827959.v1.